TECHNICAL MEMORANDUM

368

A Comparison of ETKF Targeting Guidance with ECMWF and NRL TE-SVs Targeting Guidance

S. J. Majumdar[1], C. H. Bishop[2], R. Buizza[3] and R. Gelaro[4]

Research Department

[1]University of Miami, USA
[2]The Pennsylvania State University, USA / NRL, Monterey, USA
[3]ECMWF, UK
[4]Data Assimilation Office, NASA Goddard, USA

Accepted for publication in the Quart. J. Roy. Meteorol. Soc..

(14 May 2002)

European Centre for Medium-Range Weather Forecasts
Europäisches Zentrum für mittelfristige Wettervorhersage
Centre européen pour les prévisions météorologiques à moyen terme

For additional copies please contact

The Library
ECMWF
Shinfield Park
Reading
RG2 9AX
library@ecmwf.int

Series: ECMWF Technical Memoranda

A full list of ECMWF Publications can be found on our web site under:
http://www.ecmwf.int/publications/

Abstract

Ongoing adaptive observing programs strive to improve short- and medium-range forecasts of winter weather over populated areas. Aircraft equipped with Global Positioning System (GPS) dropwindsondes are directed over ordinarily data-sparse regions (oceans) to collect observations to enhance the subsequent operational analysis-forecast cycle. Two objective techniques that have been used to identify optimal "target regions" are the Ensemble Transform Kalman Filter (ET KF) and the Singular Vector technique. The similarities and differences between targeting guidance based on the ET KF and Total Energy Singular Vectors (TESVs) are assessed for 10 cases during the NORPEX experiment. TESVs are computed at the European Centre for Medium-Range Weather Forecasts (ECMWF) and the Naval Research Laboratory (NRL) using their respective global models, and the ET KF uses 25 ECMWF ensemble perturbations.

Using measures based on (i) rankings of aircraft flight tracks and (ii) spatial similarities between targeting guidance maps, the main finding is that (a) the ET KF guidance is reasonably correlated with TESV guidance for at least 7 of the 10 NORPEX cases. Other findings include: (b) the ECMWF and NRL TESV targets sometimes differ significantly, (c) the ET KF and TESV guidance maps often display different optimal locations for targeting on smaller scales, but larger scale aspects are usually similar, (d) the ET KF generally identifies larger regions over which useful observations can be taken compared with the SV technique, and (e) regions that are deemed effective for targeting by both techniques often correspond to baroclinic zones.

The ET KF and SV techniques may identify similar regions for targeting if locations of large ensemble-based analysis error variance coincide with areas where rapid perturbation growth occurs. On the other hand, they may identify different targeting locations for the following two reasons. First, the ET KF implicitly accounts for error correlation lengthscales in its predictions of forecast error variance reduction produced by any set of targeted observations. Hence, it can identify locations for targeted observations that are distant from the regions of high analysis sensitivity that are selected for targeting by the SV technique. Second, ET KF estimates of analysis error variance are constrained to a subspace of evolved ensemble perturbations and are therefore rank-deficient.

1 Introduction

The primary aim of "adaptive sampling" or "targeting" is to improve forecasts of a weather event, by collecting observations in upstream regions where analysis errors are dynamically related to the forecast verification region of interest. During recent field programs, various objective targeting strategies have been employed to identify optimal deployments of aircraft-borne Global Positioning System (GPS) dropwindsondes over the oceans. Two such strategies are the Ensemble Transform Kalman Filter (ET KF) (Bishop *et al.* 2001) and the Singular Vector (SV) technique (Palmer *et al.* 1998). The ET KF and SV techniques are founded on different theoretical bases; however, no studies have yet been performed to identify the similarities and differences between guidance issued by the respective techniques. Especially since future adaptive observing programs and experiments are being planned (*e.g.* Toth *et al.* 2002), a thorough understanding of the targeting products issued by the two techniques would help clarify how and why the deployment of expensive observing resources would improve forecasts in some downstream area, before the observations are deployed. This paper represents a first step in comparing the versions of the ET KF and SV guidance used during targeting programs, for 10 cases from the 1998 North Pacific experiment (NORPEX).

The ET KF, which superceded the Ensemble Transform (ET) targeting technique of Bishop and Toth (1999), is currently being used at the National Centers for Environmental Prediction (NCEP) during operational Winter Storm Reconnaissance (WSR) programs (Toth *et al.* 2002). The performance of the ET and ET KF techniques during recent targeting programs is documented in Szunyogh *et al.* (1999, 2000) and Majumdar *et al.* (2001, 2002). To optimize the efficiency of the flight planning procedure at NCEP, the ET KF is used to rapidly estimate the reduction in forecast error variance within a pre-selected verification region at a future verification

time, for a number (*c.* 50) of pre-designed flight tracks. The targeted observations collected by GPS dropwindsondes released along these flight tracks are then transmitted to operational centers (along with routine observations from satellites, rawinsondes *etc.*) for use in the next analysis-forecast cycle. Typically, the decision of where to deploy the sondes must be made approximately 36 hours prior to the flight time. In addition to the flight track selection described above, the ET KF provides "summary maps" of the estimated reduction in forecast error variance within the verification region, as a function of the location in which hypothetical targeted observations are to be taken. For the comparison in this paper, we shall utilize results from both the flight track selection and summary map guidance produced by the ET KF. Further details on how these products are calculated are available in Majumdar *et al.* (2002).

The SV technique was used by the European Centre for Medium-Range Weather Forecasts (ECMWF), U.S. Naval Research Laboratory (NRL) and Météo France during the FASTEX experiment (Joly *et al.* 1999). Assessments of the performance of singular vector-based targeted observations in FASTEX are found in Montani *et al.* (1999), Langland *et al.* (1999a), Gelaro *et al.* (1999) and Bergot (1999). The SV technique was also used by NRL during NORPEX in 1998 (Langland *et al.* 1999b, Gelaro *et al.* 2000). Further information on SV-based targeting is given in Fischer *et al.* (1998), Buizza and Montani (1999) and Bergot *et al.* (1999). In addition to the SV technique, both Météo France and NRL also employed the related gradient sensitivity technique during FASTEX (Bergot 1999, Langland *et al.* 1999a).

Other targeting strategies (whose results are not shown in this paper) include those of Lorenz and Emanuel (1998), who suggest observing in regions where errors in the first guess field are large, and Pu *et al.* (1997), Pu and Kalnay (1999) who use quasi-inverse linear models to identify optimal locations for targeted observations. Reynolds *et al.* (2000), Morss *et al.* (2001) and Morss and Emanuel (2002) explored the concepts of various targeting strategies in the framework of quasi-geostrophic models. Recently, Baker and Daley (2000) developed a new adjoint-based targeting method based on observation sensitivity.

While both the SV and ET KF techniques are undergoing further development, the purpose of this paper is to compare guidance issued by the current operational version of the ET KF with SV products that were used during NORPEX. If both techniques were run simultaneously in a targeting experiment, how different would the recommended deployments of adaptive observational resources be, and how should one interpret the results?

Both techniques are described briefly in Section 2. Summary maps from the ET KF (using an ECMWF ensemble, Molteni *et al.* 1996, Buizza *et al.* 1998) and the SV techniques (generated at ECMWF and NRL) are presented in Section 3 for six NORPEX cases. Quantitative tests of the similarities between the techniques are presented in Section 4. Concluding remarks are given in Section 5.

2 The Techniques

2.1 Ensemble Transform Kalman Filter (ET KF)

For ongoing field programs and this comparison, the ET KF (Bishop *et al.* 2001) is used to solve the evolving Kalman Filter error statistics equations,

$$\begin{aligned} \mathbf{P}_q^a &= \mathbf{P}_r^a - \mathbf{P}_r^a \mathbf{H}_q^T (\mathbf{H}_q \mathbf{P}_r^a \mathbf{H}_q^T + \mathbf{R}_q)^{-1} \mathbf{H}_q \mathbf{P}_r^a, \\ \mathbf{P}_q^f &= \mathbf{M} \mathbf{P}_q^a \mathbf{M}^T + \mathbf{Q}, \end{aligned} \tag{1}$$

for Q feasible locations of a hypothetical "test-probe" of "observations". The test-probe can represent any combination of observation locations, such as the release sites of aircraft-borne dropwindsondes, or a probe of $3 \times 3 = 9$ observations at adjacent points on a 2.5° resolution grid. $\mathbf{P}_r^a$ is an estimate of the analysis error

covariance matrix associated with routine observations, and $\mathbf{P}_q^a$ is the corresponding estimate associated with routine observations plus the qth feasible probe of targeted observations. $\mathbf{H}_q$ and $\mathbf{R}_q$ are the observation operator and error covariance matrix associated with the qth probe respectively. The propagator $\mathbf{M}$ maps perturbations at the targeting time to perturbations at the later verification time, and $\mathbf{Q}$ is the covariance matrix of model errors accrued between the respective times. $\mathbf{P}_q^f$ is the forecast error covariance matrix valid at the verification time that one would obtain if all the above quantities were estimated correctly.

The ET KF uses K perturbations from operational ensemble forecasts to estimate the error covariance matrices in (1). Each perturbation is given by the difference between an individual forecast of the atmospheric state and the ensemble mean, written as a column vector of length N. These columns are then listed in a $N \times K$ matrix of raw ensemble perturbations, denoted by $\mathbf{X}$. The ET KF then uses estimates of error statistics pertaining to future hypothetical observational networks to linearly transform these perturbations via a $K \times K$ matrix $\mathbf{T}$ into a new matrix $\mathbf{Z} = \mathbf{XT}$, to produce a representative new ensemble of analyses. This same transformation is also used to produce an ensemble of perturbations, valid at a future forecast time. In the operational formulation (Majumdar *et al.* 2002), the ET KF first crudely estimates the routine analysis error covariance matrix $\mathbf{P}_r^a$ as an outer product of transformed ensemble perturbations $\mathbf{Z}_r$, *i.e.*

$$\mathbf{P}_r^a \quad = \quad \mathbf{Z}_r \mathbf{Z}_r^T \, . \tag{2}$$

The transformed perturbations are calculated via the constraint $\mathbf{Z}_r^T \, \mathbf{D}_r^{a\,-1} \mathbf{Z}_r = \mathbf{I}$, where $\mathbf{D}_r^{a\,-1}$ is a diagonal matrix listing estimates of inverse analysis error variance associated with the routine observational network, multiplied by K/N. The constraint ensures that (i) the transformed perturbations are mutually orthogonal under the norm implicit in $\mathbf{D}_r^{a\,-1}$ and that (ii) the squared amplitude of each transformed perturbation is consistent with available estimates of routine analysis error variance.

Having defined $\mathbf{P}_r^a$ in this way, (1) can then be solved rapidly for each possible location of the test-probe of targeted observations, using further transformations based on the serial assimilation theory described in Bishop *et al.* (2001). The ensemble forecast perturbations valid at the verification time are used in the estimation of the forecast error covariance matrix; no further model runs are required outside the operational ensemble. The technique yields accurate solutions to (1) provided that (a) the leading forecast error structures project onto the ensemble perturbations, (b) error covariances specified by the operational data assimilation scheme and by the ET KF are both accurate and similar, and (c) the ensemble perturbations are of sufficiently small amplitude for linear dynamics to be obeyed.

While the above conditions do not hold in practice, the ET KF has demonstrated the ability to predict the reduction in forecast error variance produced by targeted observations, during both the 2000 and 2001 WSR Programs (Majumdar *et al.* 2001, 2002). This reduction in error variance is rapidly calculated via the *signal covariance matrix* $\mathbf{S}_q^f$, defined by

$$\mathbf{S}_q^f \quad = \quad \mathbf{M} \mathbf{P}_r^a \mathbf{H}_q^T \left(\mathbf{H}_q \mathbf{P}_r^a \mathbf{H}_q^T + \mathbf{R}_q \right)^{-1} \mathbf{H}_q \mathbf{P}_r^a \mathbf{M}^T \, . \tag{3}$$

The ET KF summary maps shown in Figs 1-6 plot the sum of the diagonal values of this matrix, localized within the verification region, as a function of the centroid location of the qth feasible test-probe of targeted observations. This *signal variance* represents the estimated reduction in forecast error variance in the verification region for each test-probe location, assuming that the analysis error covariance estimates in (3) used to assimilate the observations are perfect and that linear dynamics are obeyed. We shall refer to such plots as ET KF summary maps of signal variance. The maps give an overview of the sensitivity of forecast error variance to the location of the test-probe observations. The location at which the placement of the test-probe produces the greatest signal variance is deemed optimal for targeting.

In addition to the aforementioned summary maps, the forecast signal variances associated with any number of pre-designed flight tracks consisting of likely dropwindsonde observation locations can be produced in a

similar manner. By plotting the forecast signal variance in a bar chart, for each flight track, the optimal flight track for targeting can be deduced. This technique is now used at NCEP during operational Winter Storm Reconnaissance (WSR) programs since it expedites the flight planning logistics (see Toth *et al.* 2001, Majumdar *et al.* 2002 for further details).

In this study, 25 temperature and horizontal wind perturbations from an ECMWF ensemble initialized 36 hours prior to the targeting time are used to estimate a vertically averaged "energy signal variance" for any test-probe. [1] At the time of the NORPEX experiment, the ECMWF ensemble was based on 51 members run at TL159 L31 resolution (*i.e.* spectral triangular truncation T159 with linear grid, and 31 vertical levels), with the 50 initial members produced by adding and subtracting 25 initial perturbations generated using T42L31 singular vectors optimized over 48 hours (Buizza *et al.* 1998). Our experience suggests that ET KF summary maps based on 25 or 50 independent ECMWF ensemble perturbations generally look very similar, and so we use $K = 25$ perturbations for increased computational efficiency. Note that during ongoing WSR programs, a 20-member NCEP Medium-Range Forecast (MRF) ensemble is used in addition to the 25-member ECMWF ensemble for targeting with the ET KF.

2.2 Singular Vector (SV) technique

The aim of the SV technique (Palmer *et al.* 1998) is to identify structures that grow optimally along the forecast trajectory (started at the initial time) from the targeting to the verification time. The optimization time interval (OTI) is the difference between targeting and verification times. More specifically, the idea is to target observations at the perturbations $\mathbf{z}_k$ valid at the targeting time, which evolve into the leading eigenvectors of the forecast error covariance matrix $\mathbf{P}_r^f$ associated with the routine observational network, localised within the verification region. These perturbations are called SVs. To find these vectors, one must estimate the routine analysis error covariance matrix $\mathbf{P}_r^a$ valid at the targeting time. While it is possible to make estimates of analysis error covariance identical to those assumed by the data assimilation scheme (Barkmeijer *et al.* 1998, 1999, Gelaro *et al.* 2002), in targeting experiments to date and for this comparison, the ECMWF and NRL SVs were generated under the assumption that the distribution of analysis errors is isotropic, on average, with respect to the energy norm. The SVs obtained under this assumption are called *total energy SVs* (hereafter TESVs). Practical experience shows that the spectra of the leading TESVs are at least consistent with the spectra of estimates of analysis error variance in that both have significant power in the same wavenumber range (Palmer *et al.* 1998).

Both ECMWF and NRL TESV sensitivity summaries are calculated using the same method as in Buizza and Montani (1999). The TESVs are based on forecast trajectories initialized 36 hours prior to the targeting time, and optimization time intervals specified in Table 1. Considering the jth singular vector with singular value σ_j, the initial time vertically integrated total energy $f_j(\lambda,\phi)$ is computed, where (λ,ϕ) is the gridpoint coordinate. Then, the weighted average of the total energy of the leading 4 singular vectors

$$F(\lambda,\phi) \quad = \quad \sum_{j=1}^{4} \frac{\sigma_j}{\sigma_1} f_j(\lambda,\phi) \tag{4}$$

is evaluated, and the maximum value F_{MAX} of the average total energy $F(\lambda,\phi)$ is deduced.[2] For our comparison with ET KF targets, the initial time target area Σ_{t_0} is defined by the set of gridpoints (λ,σ) where $F(\lambda,\sigma)$ is

[1] Note that this ET KF energy function differs from the total-energy norm used in SV computations (*e.g.* Buizza and Palmer 1995) since it only uses 3 levels and mean sea level pressure is not considered.

[2] As computational power increases, lower ranked SVs will be included in the future. For the purposes of this paper, the TESV computations that are practicable for operations are used.

Fig.	Case	Times				Verification Area	
		Initial	Targeting	Verification	OTI	Latitude	Longitude
	1	16/01-12	18/01-00	19/01-00	24	30-50N	135-115W
1	2	19/01-12	21/01-00	22/01-00	24	35-55N	130-110W
	3	21/01-12	23/01-00	24/01-00	24	40-60N	135-115W
2	4	23/01-12	25/01-00	26/01-12	36	32.5-52.5N	132.5-112.5W
	5	28/01-12	30/01-00	31/01-12	36	27.5-47.5N	130-110W
3	6	03/02-12	05/02-00	06/02-00	24	32.5-52.5N	135-115W
4	7	09/02-12	11/02-00	12/01-12	36	30-50N	135-115W
	8	13/02-12	15/02-00	17/02-00	48	30-50N	135-115W
5	9	18/02-12	20/02-00	21/01-12	36	30-50N	135-115W
6	10	25/02-12	27/02-00	01/03-00	48	37.5-57.5N	135-115W

Table 1: The 10 NORPEX cases used in the comparison of ET KF, ECMWF and NRL summary maps. The ECMWF ensemble perturbations used in the ET KF calculations were initialised at the initial time. The TESVs were optimized to grow along the forecast trajectory started at the initial time from the targeting to the verification time. The optimization time interval (OTI) is the difference between targeting and verification times. Times are in format day/month-hour (year is 1998).

larger than half of its maximum value,

$$\Sigma_{t_0} \quad = \quad \left\{ (\lambda, \sigma) \, | \, F(\lambda, \sigma) \geq \frac{F_{MAX}}{2} \right\}. \tag{5}$$

The weights σ_j/σ_1 have been introduced in the definition of the total-energy targeting function $F(\lambda, \sigma)$ to account for the fact that singular vectors with different ranking order grow differently. We refer to plots of the target area Σ_{t_0} in Figs 1-6 as ECMWF and NRL summary maps. The ECMWF TESVs are calculated using the tangent forward and adjoint adiabatic version of the ECMWF non-linear model with horizontal diffusion and a simple linear vertical diffusion and surface drag scheme (Buizza 1994). The NRL TESVs are computed with the same simplifications. The ECMWF TESVs are produced at T63L31 resolution, and the NRL TESVs are computed at T79L18 resolution. As shown in Gelaro *et al.* (1998) and commented on by Baker and Daley (2000), TESVs are closely related to the gradient of forecast error total energy at the verification time with respect to the analysis variables at the targeting time. Summary maps of such gradients based on energy weighted integrals of the gradient field would typically correspond quite closely to the TESV summary maps.

3 Qualitative Comparison

In this section, we present targeting summary maps from the two techniques for 6 of the more interesting NORPEX forecasting cases (refer to Table 1). Here, the purpose is to present only a qualitative assessment of the similarities and differences between the guidance produced by each technique; a quantitative assessment is presented in Section 4. Summary maps for all 10 cases can be viewed on the Website http://orca.rsmas.miami.edu/∼majumdar/comparisons/

During the NORPEX period (a warm phase of ENSO), several storms bringing unusually high precipitation made landfall on the west coast of the United States. To improve forecasts of the timing and location of these storms, targeted dropwindsondes were deployed from aircraft based in Anchorage and Honolulu between one and two days in advance of anticipated landfall. For each case, the shaded ET KF summary map is overlayed with (a) the ECMWF summary map and (b) the NRL summary map. Two relevant diagnostics, the 300hPa

Eady growth rate (Hoskins and Valdes 1990) and 850hPa vorticity, both produced from ECMWF analyses, are displayed for comparison in panels (c) and (d) respectively.

In Fig.1 (NORPEX Case 2), the optimal target locations suggested by the ECMWF and NRL TESVs are nearly identical to each other. The primary TESV maxima coincide with an amplifying baroclinic structure. The ET KF sensitivity is also high within this region. The ET KF summary also identifies another location upstream of these maxima, at 170W 40N, which coincides with a region of high low-level vorticity. The ET KF does not emphasise the region to the west of Vancouver Island, where secondary maxima of the ECMWF and NRL TESV summaries lie.

In Fig.2 (NORPEX Case 4), the ECMWF summary displays two prominent maxima, which are in similar locations to those of the ET KF. The upstream maximum is within a region of high upper-level wave amplification near 167E 38N, whereas the downstream maximum of the ET KF and ECMWF TESV summaries correspond to a region of lower amplification near 170W 35N. This downstream maximum is the primary maximum of the ECMWF TESV summary, and the NRL maximum is near this region. Note, however, that the upstream region of 167E 38N is only on the fringes of the NRL TESV summary. Furthermore, the ET KF summary indicates a minor maximum to the north-east of Hawaii, around 145W 38N. The low-level vorticity associated with a cyclone centre is high in this region. Neither TESV summary strongly emphasises this region for targeting, although they both exhibit protrusions that “point” at this feature.

Fig.3 (NORPEX Case 6) is the most clear-cut of all 10 cases, with all 3 targets closely resembling each other, coinciding with a frontal structure.

Fig.4 (NORPEX Case 7) shows elongated structures of high ET KF and ECMWF sensitivity along a large extent of the northern Pacific corresponding to the subtropical steering flow. The primary ET KF maximum coincides with a low-level vorticity maximum at 160E 37N. The NRL TESV summary (near 170-180W, 30N) is more focused than ET KF or ECMWF TESV summaries, with its maximum close to the primary ECMWF maximum in a region of high Eady growth rate associated with the subtropical jet. It is worth noting that Gelaro *et al.* (2002) produced the corresponding NRL summary for SVs based on operational estimates of analysis error variance (called VARSVs) in Fig.15 of their paper. The NRL VARSV summary exhibits a more similar shape to the more elongated structures of our ET KF and ECMWF summaries in Fig.4a.

In Fig.5 (NORPEX Case 9), both ECMWF and NRL TESV maxima are located in a similar region (around 170W, 27-35N), whereas the ET KF maximum is situated much further to the northeast, near the center of a developing cyclone. While the ET KF and TESV maxima are a large distance apart, they are all situated within an elongated zone of high wave amplification.

In Fig.6 (NORPEX Case 10), the ET KF and NRL summaries exhibit maxima in similar locations (near 165W, 45-50N), whereas the ECMWF TESV maximum is far upstream (172E 45N). The shapes of the respective TESV summaries are also very different. The main reasons why the TESV targets are so different are not obvious in this case. The ET KF maximum is situated in a region of large low-level vorticity.

A few remarks can be made upon inspecting the summary maps produced by the respective techniques:

(a) The overall structure of the TESV summaries is more localized than the shape of the ET KF summary. The ET KF shading denotes values for which the signal variance is at least 70% of the maximum possible signal variance, whereas the TESV summaries show all sites in which the weighted average of total energy is at least 50% of the maximum value (equations 4 and 5). We note that the areal coverage of the ET KF and TESV summaries depends on the threshold level; a small (large) threshold gives a large (small) area. In our study, the thresholds were chosen to ensure that both the ET KF and TESV summaries were of comparable size, and that they could be spanned by the aircraft currently used for targeting.

The fact that the ET KF summary map identifies broader target regions than the TESV summary map should not be surprising given the differences between the techniques. The ET KF attempts to predict the reduction in forecast error variance produced by any set of targeted observations, and hence ET KF summary maps combine the sensitivity to observations with estimates of analysis and forecast error covariance. Since it implicitly accounts for error correlation lengthscales in estimating error covariance matrices, the ET KF can therefore identify target locations that are distant from regions of high analysis sensitivity, especially in the vicinity of baroclinic features where error correlation lengthscales can be large. More specifically, the ET KF uses information from observations taken in distant locations to change an analysis in regions of high analysis sensitivity. It is these regions of high analysis sensitivity, from which error structures grow most rapidly into the verification region, that are identified by the TESV technique. From this point of view, it would therefore be surprising if the ET KF summary maps did not indicate a larger area over which useful observations could be taken, compared with the TESV summaries.

Furthermore, the accuracy of ET KF-based estimates of forecast error variance reduction is compromised by the rank-deficiency of the ET KF background error covariance matrix, which occurs since the number of ensemble perturbations is much less than the length of the state vector. The rank-deficiency may lead to spurious error correlations over larger distances than might be expected if background error covariances were specified accurately. Several methods have been suggested to reduce potentially spurious long-distance error correlations in ensemble-based data assimilation (Houtekamer and Mitchell 1998, 2001, Hamill and Snyder 2000, Hamill *et al.* 2001); however, no such method currently exists for ensemble-based targeting. In addition to the factors mentioned above, we also note that the breadth of the ET KF summary depends on the number and spacing of sondes in the test-probe.

(b) Although the ET KF and TESV summaries sometimes exhibit substantial differences on the small scale, the larger scale aspects often appear similar. This finding will be judged in a quantitative manner in the next section, and further discussion of this point will be deferred until after then.

(c) The summary maxima from both techniques often correspond to zones of significant wave amplification, or vorticity maxima.

(d) The NRL and ECMWF TESV summary plots exhibit significantly different target regions in 2 of the 10 cases (see the next section for further analysis). This is not surprising, since it has already been documented that TESVs are sensitive to the trajectory of the governing model (Gelaro *et al.* 1999, Buizza and Montani 1999). A comprehensive test of the variation of SV targeting summaries with the model trajectory, resolution, analysis error estimation and singular value spectrum is a subject of ongoing research, and is beyond the scope of this paper. However, such differences may be viewed as analogous, and possibly related, to those often observed in the forecasts themselves produced by different numerical weather prediction models. We also note that in cases where the forecast error is dominated by model error, targeted observations are on average likely to be of little use.

4 Quantitative Comparison

To augment the findings of our qualitative study, a quantitative comparison of the similarity between ET KF and TESV summary maps is performed, from the perspective of deciding where to deploy supplementary observational resources.[3]

[3]Due to computational and personnel changes at NRL, the data for the NRL TESV summary maps are not available. The top 50 optimal locations for targeting were derived manually from the plots, and are subject to an estimated 5% human error.

	Spearman Rank Test		Best Flight		Flatness Rank	
Case	R_s	Sig.	ET KF	ECMWF TESV	ET KF	ECMWF TESV
1	0.60	95%	I	A	2	5
2	-0.14	None	D	I	1	6
3	0.76	99%	G	J	8	9
4	0.99	99%	F	F	7	7
5	0.50	90%	I	E	6	4
6	0.81	99%	I	I	10	10
7	0.64	95%	F	F	4	3
8	0.85	99%	F	A	9	2
9	0.21	None	I	F	3	8
10	-0.52	None	A	F	5	1
Exp.	0	None				

Table 2: Columns 2-3: Spearman Rank Correlation Coefficients R_s and significance of flight track rankings, for NORPEX cases 1-10. Columns 4-5: Best ET KF and ECMWF TESV flight tracks for each case. Columns 6-7: "Flatness" (1=most flat, 10=least flat) of ET KF and ECMWF TESV flight track bar charts. Bottom row: Expected values of R_s and statistical significance if the ET KF and ECMWF TESV targeting summaries were independent.

4.1 Flight rankings of ET KF and TESV targets

The first test involves a comparison between flight tracks that would be selected by the ET KF and ECMWF TESV techniques. Ten flight tracks, identical to those used in the 2000 and 2001 Winter Storm Reconnaissance (WSR) Programs, are labeled A through J (see Fig.7). These tracks cover a limited area over the northern Pacific, compared with the large regions in which significant maxima existed on the ET KF and TESV summary maps in Figs 1-6. However, it is only these limited areas that are currently reachable by reconnaissance aircraft deployed out of Anchorage and Honolulu. The purpose of this subsection is to identify whether the selection of presently available resources for targeting is sensitive to the type of targeting strategy.

For the ET KF, the flight-ranking technique that is currently employed at NCEP during WSR programs is used; the signal variance σ_q is calculated for each of the $Q = 10$ flight tracks A,...,J, and presented in a bar chart (*e.g.* Figs 8a and 8c). In this study, the flight tracks are then ranked in order of decreasing signal variance, indicating the most effective track for targeting through to the least effective (denoted by r_q^{ETKF} for flight track q). For the ECMWF TESVs, the dropwindsonde locations for each track are projected onto the TESV summary map, and the average value of the TESVs is then calculated for each track (*e.g.* Figs 8b and 8d). The 10 flights are then ranked in decreasing order of effectiveness (denoted by r_q^{SV}). For each NORPEX case, the probability distribution-free Spearman Rank Correlation test (Wilks 1995) is then performed to determine the level of significance of the similarity between the flight rankings produced by the ET KF and SV techniques. The Spearman Rank Correlation Coefficient R_s is defined by

$$R_s \quad = \quad 1 - \frac{6\sum_{q=1}^{Q}(r_q^{\mathrm{ETKF}} - r_q^{\mathrm{SV}})^2}{Q(Q^2-1)}\,. \tag{6}$$

If there is no relationship between the two datasets, $R_s = 0$. A perfect monotonic increasing (decreasing) relationship between the rankings would give $R_s = 1$ ($R_s = -1$). The level of significance of the monotonicity is read from a table. For a 2-tailed test, the 90%, 95% and 99% levels are 0.46, 0.56 and 0.75 respectively.

The second column of Table 2 displays the value of the correlation coefficient R_s for each of the 10 NORPEX cases. The third column shows the significance level of the relationship between the flight track rankings selected by the ET KF and ECMWF SV techniques. For 7 of the 10 NORPEX cases (1,3,4,5,6,7,8), the

relationship is monotonic increasing with a $> 90\%$ level of significance. The level of significance is at least 99% for 4 of these cases. For the remaining 3 NORPEX cases (2,9,10), no monotonic increasing relationship can be deduced, and hence the flight track rankings issued by the ET KF and ECMWF SV techniques are deemed to be unrelated in these cases.

In the context of future observing experiments or programs in which variants of the ET KF and SV techniques may be used in tandem, it is important to know whether the techniques are consistent in selecting common locations for targeted observations. This is investigated in detail in the next subsection; here, the consistency between optimal flight tracks selected by the ET KF and the ECMWF TESV summaries is briefly assessed. As shown in columns 4-5 of Table 2, the optimal flight tracks selected by the ET KF and by the ECMWF TESVs coincide in just 3 of the 10 NORPEX cases (4,6,7). This result supports the observation from our qualitative comparison that the ET KF and TESV targets can differ significantly on the spatial scales over which the flight tracks vary.

The confidence in selecting the best flight with either technique can be related to the "flatness" of the bar charts, shown in Fig.8 for NORPEX cases 2 and 6. We note that the normalized ET KF bar charts are generally flatter than their TESV counterparts for all cases, as would be expected given our observations in the previous subsection that ET KF summary maps are generally broader. However, it is the flatness of a given bar chart *relative to those in other targeting cases*, using the same targeting strategy, that is important for the point we shall make here. A flat bar chart indicates that one of several flights is useful for targeting, whereas a bar chart with higher deviations discriminates between good and bad flight tracks more convincingly. To rank the flatness of ET KF and ECMWF TESV bar charts for each NORPEX case, the standard deviation is calculated for each bar chart. A relatively low (high) standard deviation indicates that the bar chart is relatively flat (not flat). The 3 NORPEX cases that on average possess the lowest flatness using both techniques are 3,4,6 (last two columns of Table 2, also see Figs 8a,b for case 6). All these cases have a 99% level of significance for the Spearman Rank test of flight track rankings. Hence, not only do the ET KF and ECMWF TESV techniques give very similar flight track rankings for these 3 cases, but the lack of flatness gives a high level of confidence in these rankings. Conversely, NORPEX cases 2 and 10 give a negative value of R_s, and they produce the flattest ET KF and ECMWF TESV bar charts respectively (see Figs 8c,d for case 2). The flat bar charts imply that the targeting techniques may not be able to distinguish between deployments of targeted observations in a reliable manner, in these two cases. While the sample size is small in this study, our preliminary results indicate that "flatness" (coupled with consistency between two targeting techniques) may be a useful measure of confidence for selecting one deployment of targeted observations over other deployments, given limited observational resources. As adaptive observing strategies and data assimilation schemes are developed further, the flatness could also potentially be used to determine the ability of different targeting strategies to assess the relative values of targeted and non-targeted observations.

4.2 Common locations of ET KF and TESV targets

The second test to quantify the correspondence between ET KF and TESV targets involves an assessment of whether the two summary maps are similar within the targeting domain of interest. There are several possible methods to compare the spatial similarity between two maps, although they all possess shortcomings for our purposes. The method selected in this paper involves the identification of common locations that each targeting technique selects as a good targeting site, and the use of a statistic similar to the Equitable Threat Score (ETS) that is used for the evaluation of quantitative precipitation forecast skill (Wilks 1995).

First, the optimal X gridpoints (on a 2.5° resolution grid) corresponding to summary maps for each targeting technique are identified. The domain from which these gridpoints are selected is the inner rectangle shown in Fig.7; a total of 561 gridpoints exists within this domain. The X gridpoints in which a test-probe of 9 targeted

	ET KF vs ECMWF SV				ET KF vs NRL SV		ECMWF SV vs NRL SV	
Case	C(50)	METS(50)	C(100)	METS(100)	C(50)	METS(50)	C(50)	METS(50)
1	12	0.04	61	0.27	22	0.18	14	0.07
2	19	0.14	68	0.36	8	-0.02	31	0.37
3	20	0.16	60	0.26	21	0.17	46	0.82
4	19	0.14	43	0.09	23	0.20	8	-0.01
5	6	-0.03	29	-0.02	22	0.18	22	0.19
6	33	0.42	75	0.46	42	0.67	36	0.50
7	3	-0.06	37	0.04	14	0.06	22	0.19
8	15	0.08	59	0.25	14	0.06	17	0.11
9	10	0.02	34	0.01	15	0.07	35	0.47
10	4	-0.05	24	-0.06	11	0.02	5	-0.04
Exp.	8.6	0.00	32.3	0.00	9.4	0.00	8.4	0.00

Table 3: Number of common gridpoints (C) and modified equitable threat scores (METS) for comparisons between the ET KF, ECMWF TESV and NRL TESV targeting techniques. Expected values of the respective scores for independent targets are given in the bottom row.

observations (centered on that gridpoint) produces the highest X values of ET KF forecast signal variance are stored, together with the gridpoints corresponding to the highest X values of each TESV summary. The number of gridpoints C common to both techniques is presented in Table 3 for each NORPEX case. For the ET KF vs ECMWF TESV comparison, the values of C corresponding to $X = 50$ and $X = 100$ are tabulated in columns 2 and 4 of Table 3, respectively. For example, for the top $X = 50$ targeting locations selected by each of the ET KF and ECMWF TESV techniques for NORPEX Case 1, $C = 12$ locations were in the top 50 for both techniques. For $X = 50$, the values of C for the (i) ET KF vs NRL TESV and (ii) ECMWF TESV vs NRL TESV comparisons are listed in columns 6 and 8 of Table 3 respectively.

Next, to assess whether these numbers of common gridpoints between two targeting techniques are significant, we use a statistic that we shall call the Modified Equitable Threat Score (METS), which we define as

$$\text{METS} = \frac{C - E(C)}{2X - C - E(C)} \tag{7}$$

where $E(C)$ is the expected number of common locations between the techniques, averaged over all feasible realizations of summary maps produced by each technique. The selection of $E(C)$ is non-trivial, since the ET KF and TESV techniques both tend to identify clusters of targeting locations rather than a set of gridpoints that are not spatially correlated with one another. Our method for calculating $E(C)$ is described in the Appendix. The values of METS are then calculated for each NORPEX case using (7), comparing (i) ET KF vs ECMWF TESV targets for $X = 50$ and $X = 100$, (ii) ET KF vs NRL TESV targets for $X = 50$ and (iii) ECMWF TESV vs NRL TESV targets for $X = 50$. A METS value greater than (less than) zero implies that a larger (smaller) number of common gridpoints between the targeting techniques' summaries exists than by pure chance. Hence, a positive value of METS would imply that the targets are related; the larger the value of METS, the more closely related are the distributions of the optimal 50 gridpoints selected by each technique. If both sets of 50 gridpoints are identical (*i.e.* $C = X = 50$), METS=1. One minor shortcoming of the METS statistic (and the original ETS statistic) is that the value is not -1 when the number of common locations is zero, and hence an interpretation of the magnitude of negative values of METS is not transparent. We note that while the METS score is objective, our judgement of the strength of correspondence between two maps is somewhat subjective.

For $X = 50$, the METS score for the ET KF vs ECMWF TESV comparison is positive for 7 of the 10 NORPEX cases (1,2,3,4,6,8,9), and negative for the other three (5,7,10) (Column 3 of Table 3). As expected from Figs

	ET KF vs Eady		ET KF vs Vort		ET KF vs A.E.Var		ECMWF vs Eady		NRL vs Eady	
Case	C(50)	METS	C(50)	METS	C(50)	METS	C(50)	METS	C(50)	METS
1	7	-0.01	4	-0.01	4	-0.03	18	0.15	3	-0.03
2	5	-0.03	9	0.05	14	0.10	12	0.07	6	0.00
3	10	0.03	3	-0.02	6	0.00	11	0.05	10	0.05
4	17	0.12	8	0.03	20	0.19	10	0.04	14	0.10
5	1	-0.08	9	0.05	19	0.17	13	0.08	9	0.04
6	6	-0.02	3	-0.02	18	0.15	8	0.02	6	0.00
7	14	0.08	10	0.06	21	0.20	11	0.05	9	0.04
8	11	0.04	8	0.03	20	0.19	12	0.07	7	0.01
9	32	0.40	9	0.05	19	0.17	10	0.04	14	0.10
10	4	-0.04	20	0.20	22	0.22	18	0.15	8	0.03
Exp.	7.9	0.00	5.0	0.00	6.4	0.00	6.5	0.00	5.7	0.00

Table 4: Number of common gridpoints between the top 50 sites selected by the targeting techniques, and the top 50 respective values of Eady growth rate and low-level vorticity. Expected values of the respective scores are given in the last row.

1-6, the value of METS is highest for NORPEX Case 6 (Fig.3). Comparing these results with those for the flight track rankings in the previous subsection, we note that both quantitative tests identify a reasonable degree of similarity between the ET KF and ECMWF TESV targets for cases 1,3,4,6,8. For cases 2,5,7,9, one of the two tests suggests that the ET KF and ECMWF TESV summaries are similar. Neither test suggests that the summaries are similar in Case 10, which is as expected upon inspection of Fig.6.

The values of METS are also calculated for $X = 100$, where the expected number of common gridpoints between ET KF and ECMWF TESV summaries is 32.3 out of 100. For NORPEX cases 1,2,3,7,8, the METS has increased significantly, compared with when $X = 50$ (see columns 3 and 5 of Table 3). In the other 5 cases, the METS changed by no more than 0.05. Hence, we suggest that the ET KF and ECMWF TESV targeting summaries possess, on average, a higher degree of similarity on the larger scales than on the smaller scales.

For $X = 50$, the ET KF and NRL TESVs exhibit a positive METS for 9 of the 10 NORPEX cases.

The final two columns of Table 3 show the number of common gridpoints and the METS values for the ECMWF TESV summaries versus the NRL SV summaries. As might be expected, there is a high degree of correspondence between the two respective TESV summaries for some cases (especially 2,3,6,9), and in general, the two TESV summaries are more similar to each other than to the ET KF summary (with a couple of exceptions).

Similar tests were performed to identify quantitatively whether the ET KF and TESV techniques bore any relation to the ECMWF 300hPa Eady growth rate, plotted in panel (c) of Figs 1-6. Results are shown in Table 4; the most consistent result we found is that the ECMWF and NRL TESV summaries generally exhibited a reasonable level of correlation to the Eady growth rate for most NORPEX cases. This result is to be expected since SVs often tend to identify regions of (potentially) strong baroclinic instability. The NRL TESVs usually compared favourably to the Eady growth rate, although not to the extent of the ECMWF TESVs. Since the Eady growth rate was derived using ECMWF analyses, one might expect the ECMWF TESVs to be more closely related to it than the NRL TESVs. In 5/10 cases, the ET KF summaries were deemed to bear a reasonable level of correspondence with the Eady growth rate (most notably, NORPEX case 9, see Fig.5).

Comparing the ET KF summaries with the ECMWF derived 850hPa vorticity field, a usually weak but positive METS value was found in 7/10 cases (NORPEX case 10 being a standout case, see Fig.6). No systematic correspondence was found between either of the TESV summaries and the low-level vorticity (results not shown). For more comprehensive insights into relationships between evolving singular vectors and the atmospheric

flow, the interested reader is referred to Reynolds *et al.* (2001) and Morgan (2001).

The relationship between ET KF summaries and the predicted ensemble-based routine analysis error variance at the targeted observing time, given by the vertically averaged diagonal terms in (2), is also tested. Reading from columns 6 and 7 of Table 4, we notice that the ET KF targets often, but not always, correspond to regions of high routine analysis error variance. Hence, ET KF targets can locate regions in which rapidly growing errors are dynamically connected to the verification region, or regions in which the analysis error is likely to be high upstream of the verification region. In the latter scenario, errors in the upstream region need not be growing rapidly; as long as they are correlated with forecast errors within the verification region at the verification time, the ET KF would pick such locations as viable for targeting. Of course, locations in which (i) the predicted routine analysis error variance is large, (ii) errors are growing rapidly, and (iii) errors are dynamically correlated with those in the verification region, stand the best chance of being selected by the ET KF for targeting (for example, NORPEX cases 4,7,9).

5 Concluding Remarks

A qualitative and quantitative comparison between targeting guidance produced by the Ensemble Transform Kalman Filter (ET KF), and the ECMWF and NRL Total Energy Singular Vectors (TESVs) has been performed for 10 forecast cases of the NORPEX field experiment. Two objective criteria have been defined to assess the similarity between the targets, based on (i) the practical problem of identifying the optimal flight path for targeting, and (ii) a comparison of patterns between the respective (vertically integrated) targeting summary maps. Targets provided by two different techniques are considered to be similar if (i) the Spearman Rank Correlation Coefficient $R_s > 0.46$ ($> 90\%$ significance) for flight path rankings, and (ii) the Modified Equitable Threat Score (METS) is positive for summary maps. Generally speaking, results based on these two criteria have indicated that:

(a) Based on criterion (i), the flight track rankings produced by the ET KF and ECMWF TESVs are well-correlated for 7/10 NORPEX cases. Based on criterion (ii), the ET KF and ECMWF TESV summary maps are similar in 7/10 NORPEX cases, and the ET KF and NRL TESV summary maps are similar in 9/10 NORPEX cases.

(b) ECMWF and NRL SV targets differ in 2/10 NORPEX cases (METS < 0)

(c) The ET KF and TESV summary maps often exhibit differences on smaller scales, whereas the larger scale aspects are usually quite similar.

(d) The ET KF summary maps generally indicate that the region over which targeted observations should be taken is larger than that identified by the SV summary maps.

(e) Summary map maxima from both techniques sometimes correspond to baroclinic zones in which upper-level wave amplification is occurring, or where the low-level vorticity is large.

Both the “flight ranking” and “summary map” criteria demonstrated that the ET KF, ECMWF TESV and NRL TESV maxima were related in a majority of cases. However, there is some sensitivity to the selected criterion: for example, in NORPEX Case 2 (Fig.1), the targeting techniques exhibited very different targets from the perspective of a flight planner, whereas the summary map criterion demonstrated a high level of similarity between the techniques. While the ET KF and SV techniques were deemed to produce similar results using both evaluation methods for 5 NORPEX cases (1,3,4,6,8), in only one case (10) were the summaries produced by the two techniques found to be completely unrelated. As expected, the NRL TESV summaries generally possessed a higher degree of similarity to the ECMWF TESV summaries than the ET KF summaries, comparing

the relative METS scores. Nonetheless, the NRL TESV summaries and the ET KF summaries did exhibit a reasonable level of correspondence, considering the differences between the targeting strategies and model trajectories. It was also suggested that the reliability of a targeting strategy in identifying an optimal deployment of targeted observations can be estimated via a measure of the "flatness" of charts used to discriminate between different feasible deployments.

To understand our result (a), that the ET KF summary map does not often select a profoundly different region to the TESV summary maps, recall the work of Farrell (1984, 1988, 1989) and Buizza and Palmer (1995). They pointed out that perturbation growth increases as factors such as baroclinicity and vertical and horizontal wind shear increase; in other words, rapid perturbation growth is enhanced near large unstable gradients in the mass-momentum field. Since individual members of ensemble forecasts typically disagree about the precise horizontal location of such large gradients, large gradient regions typically correspond to higher levels of ensemble spread and hence to higher ensemble-based estimates of analysis error variance. For this reason, one might speculate that atmospheric regions supporting rapid growth would correspond to regions where the ET KF estimate of analysis error variance is large. Thus, provided the ET KF is applied to an ensemble large enough to distinguish the areas of ensemble spread that are most closely linked dynamically to the verification region, one would not expect the dependence of the ET KF results on ensemble-based analysis error variance to force the ET KF sensitivity summary to look profoundly different to the SV sensitivity summary.

The result (b) that the ECMWF and NRL TESV summaries sometimes differ is not unexpected, bearing in mind the results of Buizza and Montani (1999) and Gelaro *et al.* (1999) who demonstrated the variability of SV structures with model trajectory.

Our finding (c) that the ET KF and TESV summaries sometimes differ significantly on smaller scales might be expected, since the ET KF uses spatially-varying, flow-dependent estimates of the analysis error covariance matrix whereas the targeted TESVs used in this paper assume a spatially-invariant analysis error covariance matrix. The assumption of horizontally homogeneous analysis error (implicit in the choice of the total energy norm) means that the TESV summary maps highlight regions of the atmosphere that are dynamically connected to the verification region and would support rapid error growth. The spatially (and temporally) varying nature of the analysis error variance estimated by the ET KF, however, implies that a region in which the estimated analysis error variance is large and the error growth rate is moderate could be selected by the ET KF as a preferable region to take observations than one associated with higher perturbation growth rates. Furthermore, since analysis sensitivities are smoothed out to the lengthscales of error correlation assumed by the ET KF data assimilation scheme, it is also not surprising to see a lack of agreement between the two techniques at small scales. This conclusion leads us to ask whether there are any dynamically important lengthscales beyond which one would expect the ET KF and SV targets to agree, and below which one would expect significant differences between the targets.

Our observation (d) that ET KF summaries are generally broader than the TESV summaries stems from different assumptions implicit in the two techniques. The ET KF accounts for error correlation lengthscales in the routine analysis error covariance matrix in predicting the sensitivity of forecast error variance reduction to deployments of targeted observations. Hence it acts to spread observational information into areas where errors are highly correlated with those at the observation locations. On the other hand, the TESV identifies regions of high analysis sensitivity, from which errors grow most rapidly into the verification region. Furthermore, the limited ensemble size used in the ET KF leads to a rank-deficiency problem, in which spurious large-scale error covariances may be produced. The lengthscale exhibited in the ET KF summary is also dependent on the areal coverage of the hypothetical "test-probe".

While our remark (e) that both ET KF and TESV targets often coincide with regions of high baroclinicity is neither new (see Szunyogh *et al.* 2000 and Reynolds *et al.* 2001) nor unexpected, it supports an argument for

further *in-situ* targeted observing. Upon inspection of archived GOES-9 infrared satellite imagery (not shown in this paper), these baroclinic regions are sometimes cloudy, which again is not surprising. The detailed vertical structure of the atmosphere sampled by dropwindsondes deployed in judiciously chosen target regions may therefore augment routinely available satellite observations in the analysis and prediction of weather features such as fronts and jet streams. Further research is required to determine whether an optimal mix of *in-situ* and remotely sensed observations would improve an analysis-forecast cycle significantly, using a state-of-the art data assimilation scheme.

This paper represents a first attempt towards understanding the similarities and differences between two objective strategies that were used during recent targeting campaigns. Both the ET KF and SV techniques are undergoing further development in research mode, for use in future observing programs. In particular, the estimation of the analysis error covariance matrix valid at the targeting time requires improvement in both techniques. Several difficulties present themselves, such as the fact that flow-dependent analysis error covariances are unavailable prior to the targeting time. The currently crude ET KF estimation of analysis error covariance, assuming that routine observations are taken globally at intervening times up to and including the targeting time, first needs to be refined via a rescaling parameter, using a technique such as that of Dee (1995). Moreover, the realism of ensemble-based estimates of routine analysis error covariance structures needs to be evaluated.

Recent efforts to improve estimation of the analysis error covariance metric used in SV computations have been made. Barkmeijer *et al.* (1998, 1999) proposed the use of Hessian SVs (HSVs) associated with the true routine analysis error covariance matrix. These HSVs produce the theoretically optimal estimate of the forecast error covariance matrix (Houtekamer 1995, Ehrendorfer and Tribbia 1997) associated with the routine analysis error covariance matrix. Since the ET KF uses the Kalman filter error statistics equations to estimate the effect of any deployment of targeted observations on forecast error covariance reduction, the HSVs would in theory represent the ideal set of ensemble perturbations upon which to apply the ET KF, if an optimal data assimilation scheme were being used. However, present specifications of background error covariances are far from optimal and, furthermore, calculations of HSVs are not yet computationally feasible in the timeframes under which adaptive observing programs operate.

Recently, Gelaro *et al.* (2002) proposed an alternative specification of the analysis error covariance metric, which is consistent with operational, flow-dependent estimates of analysis error variance associated with the routine observational network. The corresponding SVs, termed variance SVs (VARSVs), represent a potentially feasible method for selecting locations for targeted observations. As described in Gelaro *et al.* (2002), the optimal targeting sites selected by the VARSVs can often be in different locations to those selected by TESVs computed using an identical model, although the general structure of the respective SV summaries is fairly similar. Moreover, Gelaro *et al.* (2002) found that the VARSV summaries tended more to emphasize locations in which the analysis error was expected to be large, compared with the targeting summaries of the TESVs that assume an average isotropic distribution of analysis errors. One might therefore expect the optimal targeting locations selected by the ET KF to be more similar to those chosen by the VARSVs than those chosen by the TESVs.

The results of this paper ought to be interpreted with the knowledge that both ET KF and SV targets are liable to vary if one adjusts the estimates of analysis error covariance associated with the routine observational network at the targeting time. Such estimates are currently far from optimal. Modifying these estimates, together with an improved theoretical understanding of how the ET KF, analysis SV and observation-sensitivity based targeting schemes (*e.g.* Baker and Daley 2000) are related, are topics of ongoing research.

Acknowledgements

Sharanya Majumdar and Craig Bishop gratefully acknowledge the contributions of Zoltan Toth and Istvan Szunyogh in implementing the ET KF technique in adaptive observing programs, and also financial support of NSF Grants ATM 96-12502 and ATM 98-14376. Sharanya Majumdar is grateful for financial support from NOAA Grant NA67RJ0149. Craig Bishop received support under ONR Project Element 0601153N, Project Number BE-033-0345 and also ONR Grant number N00014-00-1-0106. The authors also acknowledge the support and encouragement of Alan J. Thorpe and Andrea Montani in the early stages of this work. Finally, the authors are grateful to two anonymous reviewers for their constructive comments and criticisms which helped improve the manuscript.

Appendix: calculation of $E(C)$

The term $E(C)$ represents the expected number of common locations between two summary maps, averaged over all feasible realizations of summary maps produced by each technique. The ET KF and TESV summary maps both tend to exhibit areas that are favourable for targeting rather than a random scatter of gridpoints that are not spatially correlated with one another. In other words, if a particular gridpoint is selected by the targeting technique, it is more likely that the technique would choose other gridpoints close to it for targeting, rather than gridpoints (say) 3000km away from it. Moreover, the zonal and meridional scales of the ET KF and TESV targets are different, as is observed from the qualitative comparison in Section 3. With these concerns in mind, one cannot simply calculate $E(C)$ by assuming that each technique selects its gridpoints in a purely random manner, or that some fixed correlation lengthscale is associated with the techniques. Instead, $E(C)$ is estimated empirically by assuming that data from the summary maps for all 10 NORPEX cases are all equally likely realizations of a stochastic process.

For the ET KF vs ECMWF TESV comparison, the number of common gridpoints between the ET KF summary for NORPEX case 1 and each ECMWF TESV summary for NORPEX cases 2-10 is calculated. The average over these 9 values, which we shall call E_1, is then taken. E_2 is found in a similar manner, averaging the number of common gridpoints between the ET KF summary for NORPEX case 2 and the ECMWF TESV summaries for the unrelated NORPEX cases $1,3,4,\ldots,10$. Values for $E_3,\ldots,E_{10}$ are also calculated in this fashion. The expected number of common gridpoints between the ET KF and ECMWF TESV summaries, based on 90 assumed random (but not totally independent) realizations, is then the average of $E_1,\ldots,E_{10}$. The value of $E(C)$ is 8.6, *i.e.* given that the ET KF and ECMWF SV summaries generally exhibit particular shapes, one would expect that between 8-9 common gridpoints would be found if the top 50 targeting locations were selected by each technique, and their respective summary maps were unrelated. Similarly, values of $E(C)$ are calculated for comparisons between summary maps for other combinations of techniques. Generally speaking, the larger the common lengthscale between two techniques, the larger the value of $E(C)$. For example, if both techniques randomly selected each of the top 50 gridpoints for targeting with no spatial correlation, $E(C) = 4.4$. Our test using these empirically derived values of $E(C)$ for each pair of techniques is more rigorous, and also more stringent, than assuming that all gridpoints are uncorrelated and equally likely locations for targeted observing.

References

Baker, N. L. and Daley, R. 2000 Observation and background adjoint sensitivity in the adaptive observation-targeting problem. *Quart. J. Roy. Meteor. Soc.,* **126,** 1431-1454

Barkmeijer, J., van Gijzen, M and Bouttier, F. 1998 Singular vectors and estimates of the analysis error covariance metric. *Quart. J. Roy. Meteor. Soc.,* **124,** 1695-1713

Barkmeijer, J., Buizza, R and Palmer, T. N. 1999 3d-Var Hessian singular vectors and their potential use in the ECMWF Ensemble Prediction System. *Quart. J. Roy. Meteor. Soc.,* **125,** 2333-2351

Bergot, T. 1999 Adaptive observations during FASTEX : a systematic survey of upstream flights. *Quart. J. Roy. Meteor. Soc.,* **125,** 3271-3298

Bergot, T., Hello, G., Joly, A. and Malardel, S. 1999 Adaptive observations : A feasibility study. *Mon. Wea. Rev.,* **127,** 743-765

Bishop, C.H. and Toth, Z. 1999 Ensemble transformation and adaptive observations. *J. Atmos. Sci.,* **56,** 1748-1765

Bishop, C. H., Etherton, B. J. and Majumdar, S. J. 2001 Adaptive Sampling with the Ensemble Transform Kalman Filter Part I : Theoretical Aspects. *Mon. Wea. Rev.,* **129,** 420-436.

Buizza, R. 1994 Sensitivity of optimal unstable structures. *Quart. J. Roy. Meteor. Soc.,* **120,** 429-451

Buizza, R. and Palmer, T. N. 1995 The singular-vector structure of the atmospheric global circulation. *J. Atmos. Sci.,* **52,** 1434-1456

Buizza, R., Petroliagis, T., Palmer, T. N., Barkmeijer, J., Hamrud, M., Hollingsworth, A., Simmons, A., and Wedi, N. 1998 Impact of model resolution and ensemble size on the performance of an ensemble prediction system. *Quart. J. Roy. Meteor. Soc.,* **124,** 1935-1960

Buizza, R. and Montani, A. 1999 Targeted Observations using Singular Vectors. *J. Atmos. Sci.,* **56,** 2965-2985

Dee, D. 1995 On-line estimation of error covariance parameters for atmospheric data assimilation. *Mon. Wea. Rev.,* **123,** 1128-1145

Ehrendorfer M. and Tribbia, J. J. 1997 Optimal prediction of forecast error covariances using singular vectors. *J. Atmos. Sci.,* **54,** 286-313

Farrell, B. F. 1984 Modal and non-Modal Baroclinic Waves. *J. Atmos. Sci.,* **41,** 668-673

Farrell, B. F. 1988 Optimal Excitation of Neutral Rossby Waves. *J. Atmos. Sci.,* **45,** 163-172

Farrell, B. F. 1989 Optimal Excitation of Baroclinic Waves. *J. Atmos. Sci.,* **46,** 1193-1206

Fischer, C., Joly, A. and Lalaurette, F. 1998 Error growth and Kalman Filtering within an idealized baroclinic flow. *Tellus*, **50A,** 596-615

Gelaro, R., Buizza, R., Palmer, T. N. and Klinker, E. 1998 Sensitivity analysis of forecast errors and the construction of optimal perturbations using singular vectors. *J. Atmos. Sci.,* **55,** 1012-1037

Gelaro, R., Langland, R. H., Rohaly, G. D. and Rosmond, T. E. 1999 An assessment of the singular vector approach to targeted observing using the FASTEX data set. *Quart. J. Roy. Meteor. Soc.,* **125,** 3299-3328

Gelaro, R., Reynolds, C. A., Langland, R. H. and Rohaly, G. D. 2000 A predictability study using geostationary satellite wind observations during NORPEX. *Mon. Wea. Rev.,* **128,** 3789-3807

Gelaro, R., Rosmond, T.E., and Daley, R. 2002 Singular vector calculations with an analysis error variance metric. *Mon. Wea. Rev.,* **130,** 1166-1186

Hamill, T. M. and Snyder, C. 2000 A hybrid ensemble Kalman filter / 3d-variational analysis scheme. *Mon. Wea. Rev.,* **128,** 2905-2919

Hamill, T. M., Whitaker, J. S. and Snyder, C. 2001 Distance-dependent filtering of background error covariance estimates in an ensemble Kalman filter. *Mon. Wea. Rev.,* **129,** 2776-2790

Hoskins, B. J. and Valdes, P. J. 1990 On the existence of storm-tracks. *J. Atmos. Sci.,* **47,** 1854-1864

Houtekamer, P. L.. 1995 The construction of optimal perturbations. *Mon. Wea. Rev.,* **123,** 2888-2898

Houtekamer, P. L. and Mitchell, H. L. 1998 Data assimilation using an ensemble Kalman filter technique. *Mon. Wea. Rev.,* **126,** 796-811

Houtekamer, P. L. and Mitchell, H. L. 2001 A sequential ensemble Kalman filter for atmospheric data assimilation. *Mon. Wea. Rev.,* **129,** 123-137

Joly, A. and CoAuthors 1999 Overview of the field phase of the Fronts and Atlantic Storm-Track EXperiment (FASTEX) project. *Quart. J. Roy. Meteor. Soc.,* **125,** 3131-3164

Langland, R. H., Gelaro, R., Rohaly, G. D. and Shapiro, M. A. 1999a Targeted observations in FASTEX : Adjoint-based targeting procedures and data impact experiments in IOP17 and IOP18. *Quart. J. Roy. Meteor. Soc.,* **125,** 3241-3270

Langland, R. H. and Coauthors 1999b The North Pacific Experiment (NORPEX-98) : Targeted Observations for Improved North American Weather Forecasts. *Bull. Amer. Meteor. Soc.,* **80,** 1363-1384

Lorenz, E. N. and Emanuel, K. A. 1998 Optimal sites for supplementary weather observations : Simulation with a small model. *J. Atmos. Sci.,* **55,** 399-414

Majumdar, S. J., Bishop, C. H., Etherton, B. J. Szunyogh, I. and Toth, Z. 2001 Can an Ensemble Transform Kalman Filter predict the reduction in forecast-error variance produced by targeted observations? *Quart. J. Roy. Meteor. Soc.,* **127,** 2803-2820

Majumdar, S. J., Bishop, C. H., Etherton, B. J. and Toth, Z. 2002 Adaptive Sampling with the Ensemble Transform Kalman Filter Part II : Field Program Implementation. *Mon. Wea. Rev.,* **130,** 1356-1369

Molteni, F., Buizza, R., Palmer, T. N. and Petroliagis, T. 1996 The ECMWF ensemble prediction system : methodology and validation. *Quart. J. Roy. Meteor. Soc.,* **122,** 73-120

Montani, A., Thorpe, A. J., Buizza, R. and Undén, P. 1999 Forecast skill of the ECMWF model using targeted observations during FASTEX. *Quart. J. Roy. Meteor. Soc.,* **125,** 3219-3240

Morgan, M. C. 2001 A potential vorticity and wave activity diagnosis of optimal perturbation evolution. *J. Atmos. Sci.,* **58,** 2518-2544

Morss, R. E., Emanuel, K. A. and Snyder, C. 2001 Idealized adaptive observation strategies for improving numerical weather prediction. *J. Atmos. Sci.,* **58,** 210-234

Morss, R. E. and Emanuel, K. A. 2002 Influence of added observations on analysis and forecast errors: Results from idealized systems. *Quart. J. Roy. Meteor. Soc.,* **128,** 285-322

Palmer, T. N., Gelaro, R., Barkmeijer, J. and Buizza, R. 1998 Singular vectors, metrics, and adaptive observations *J. Atmos. Sci.,* **55,** 633-653

Pu, Z., Kalnay, E., Sela, J. and Szunyogh, I. 1997 Sensitivity of forecast error to initial conditions with a quasi-inverse linear method. *Mon. Wea. Rev.,* **125,** 2479-2503

Pu, Z. and Kalnay, E. 1999 Targeting observations with the quasi-inverse linear and adjoint NCEP global models: Performance during FASTEX. *Quart. J. Roy. Meteor. Soc.,* **125,** 3329-3338

Reynolds, C. A., Gelaro, R. and Palmer, T. N. 2000 An examination of targeting methods in a simplified setting. *Tellus,* **52A,** 391-411

Reynolds, C. A., Gelaro, R. and Doyle, J. 2001 Relationship between singular vectors and transient features in the background flow. *Quart. J. Roy. Meteor. Soc.,* **127,** 1731-1760

Szunyogh, I., Toth, Z., Emanuel, K. A., Bishop, C. H., Snyder, C., Morss, R. E., Woolen, J. S. and Marchok, T. P. 1999 Ensemble-based targeting during FASTEX : the impact of dropsonde data from the LEAR jet. *Quart. J. Roy. Meteor. Soc.,* **125,** 3189-3217

Szunyogh, I., Toth, Z., Morss, R. E., Majumdar, S. J., Etherton, B. J. and Bishop, C. H. 2000 The effect of targeted dropsonde observations during the 1999 Winter Storm Reconnaissance Program. *Mon. Wea. Rev.,* **128,** 3520-3537

Toth, Z., Szunyogh, I., Bishop, C. H., Majumdar, S. J., Morss, R. E. and Lord, S. J. 2001 On the use of targeted observations in operational numerical weather prediction. *Preprints of the 5th AMS Symposium on Integrated Observing Systems, Albuquerque NM, 15-19 January 2001,* 72-79

Toth, Z. and Coauthors 2002 Adaptive observations at NCEP: Past, present and future. *Preprints of the Symposium on Observations, Data Assimilation and Probabilistic Prediction, Orlando FL, 13-17 January 2002,* 185-190

Wilks, D. S. 1995 *Statistical Methods in the Atmospheric Sciences: An Introduction.* International Geophysics Series, **59,** Academic Press, 464 pp.

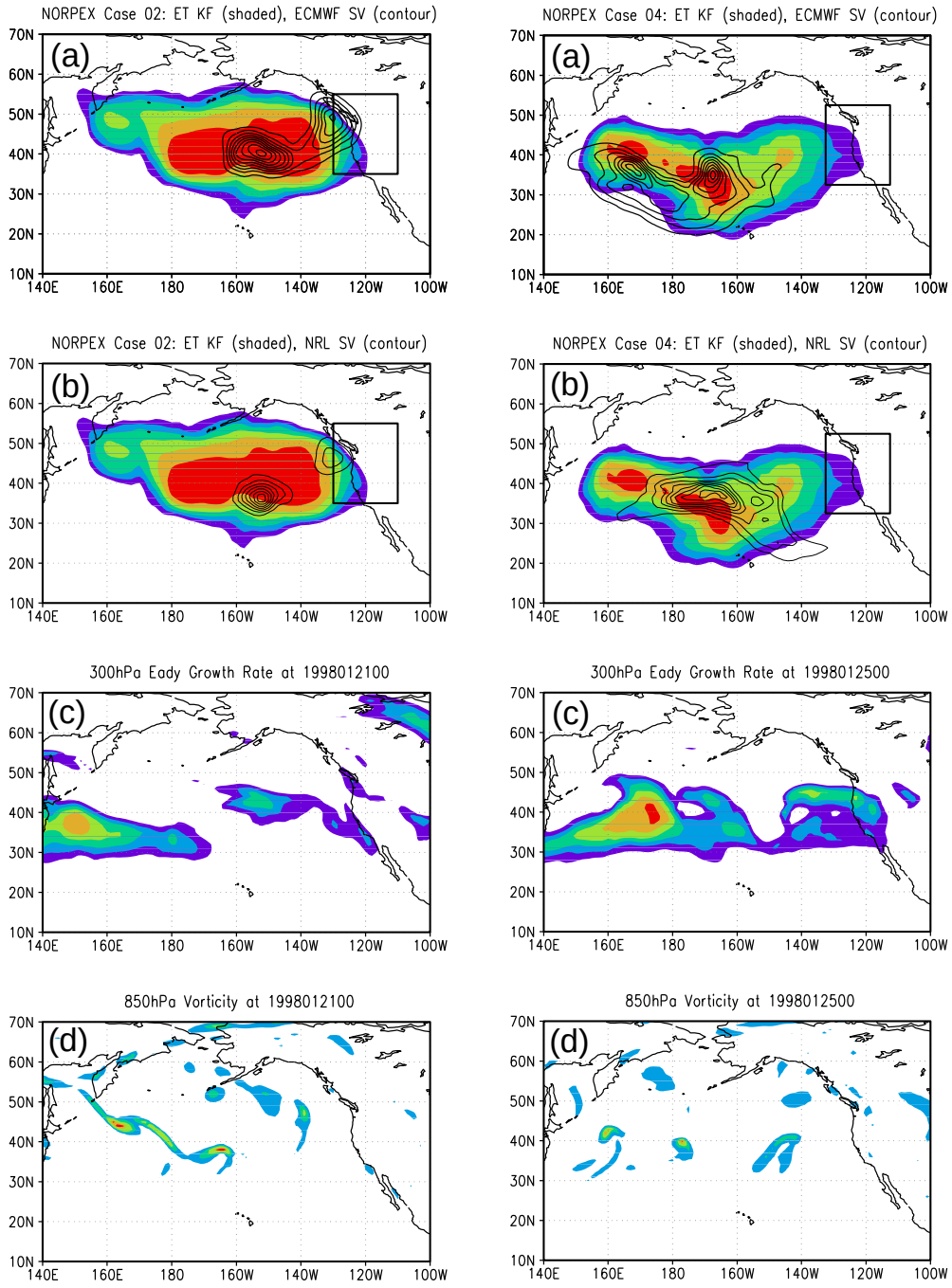

Figure 1: (left). (a) Shading: ET KF summary map for targeting at 00 UTC, 21 Jan 1998, verification 00 UTC, 22 Jan 1998. Shading increments are 5% of the ET KF maximum, from 70-75% (lightest shade) to 95-100% (darkest). Contour: ECMWF TESV summary map for the same case. Rectangular verification region over the western United States is shown. (b) Shading: as in (a). Contour: NRL SV summary map for the same case. (c) ECMWF 300hPa Eady growth rate at the targeting time. (d) ECMWF 850hPa vorticity analysis at the targeting time (positive vorticity greater than 10% of the maximum vorticity).

Figure 2: (right). Targeting 00UTC, 25 Jan 1998, verification 12UTC, 26 Jan 1998.

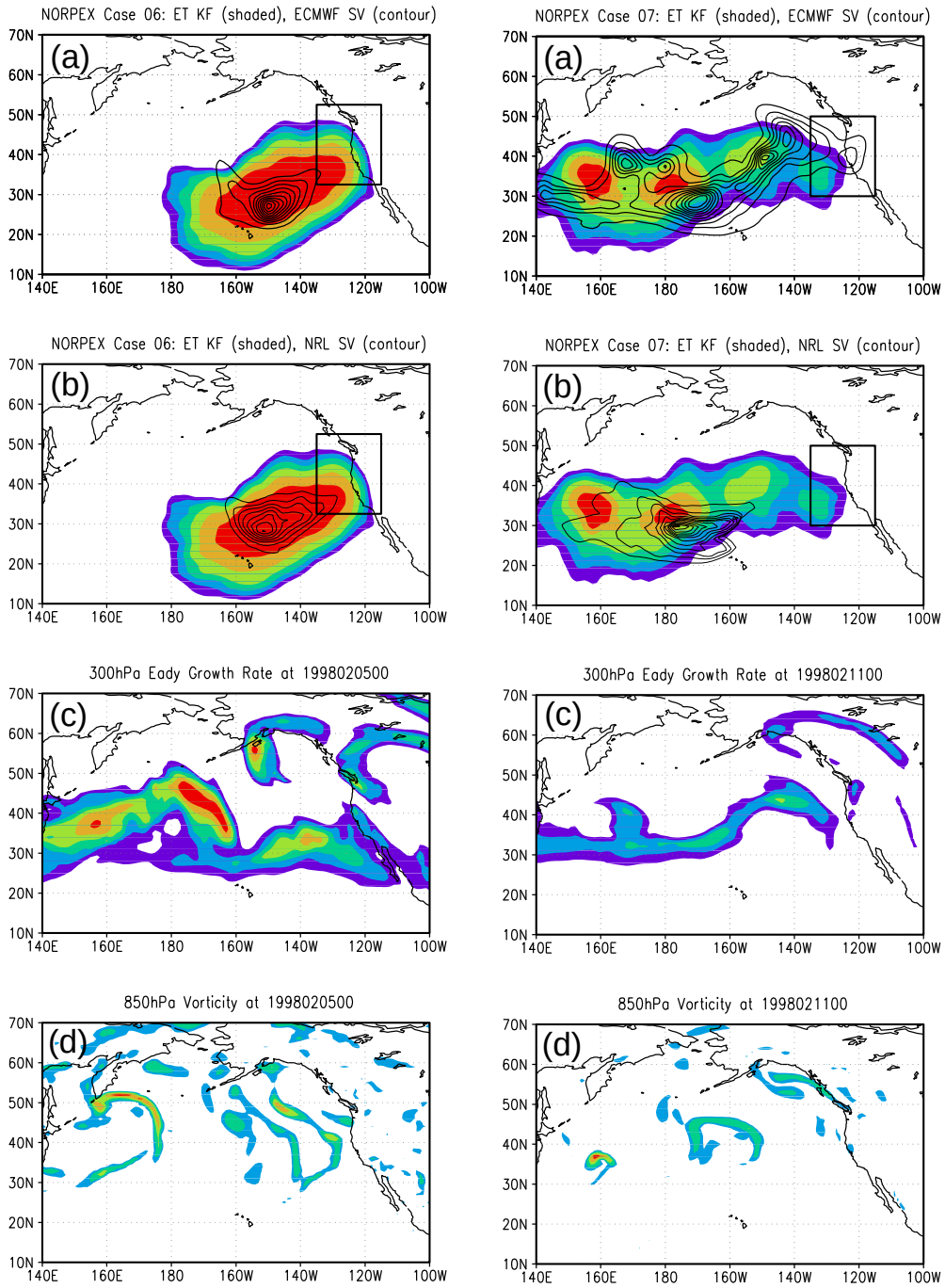

Figure 3: (left). Targeting 00 UTC, 5 Feb 1998, Verification 00 UTC, 6 Feb 1998.

Figure 4: (right). Targeting 00 UTC, 11 Feb 1998, Verification 12 UTC, 12 Feb 1998.

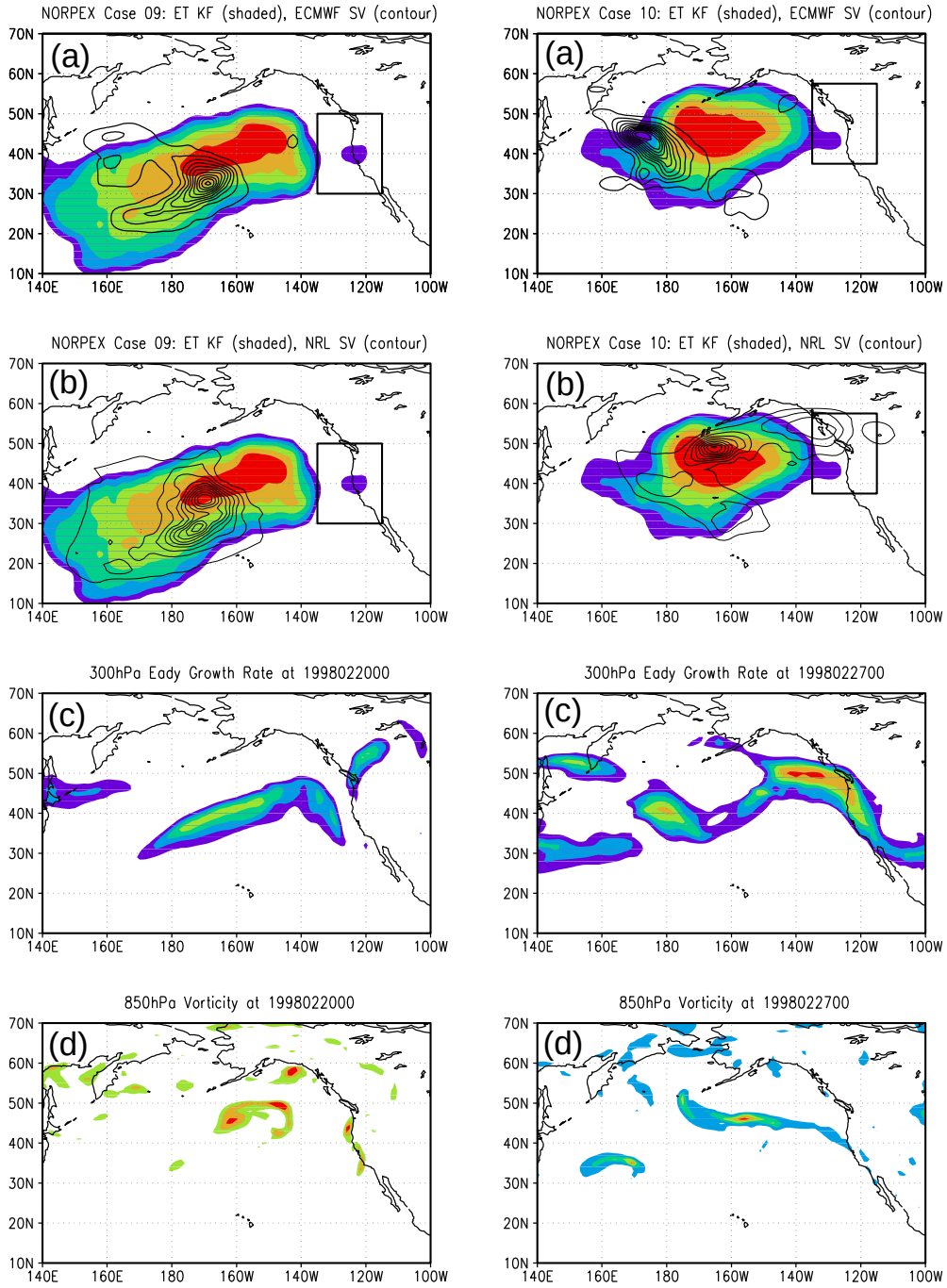

Figure 5: (left). Targeting 00 UTC, 20 Feb 1998, Verification 12 UTC, 21 Feb 1998.

Figure 6: (right). Targeting 00 UTC, 28 Feb 1998, Verification 00 UTC, 01 Mar 1998.

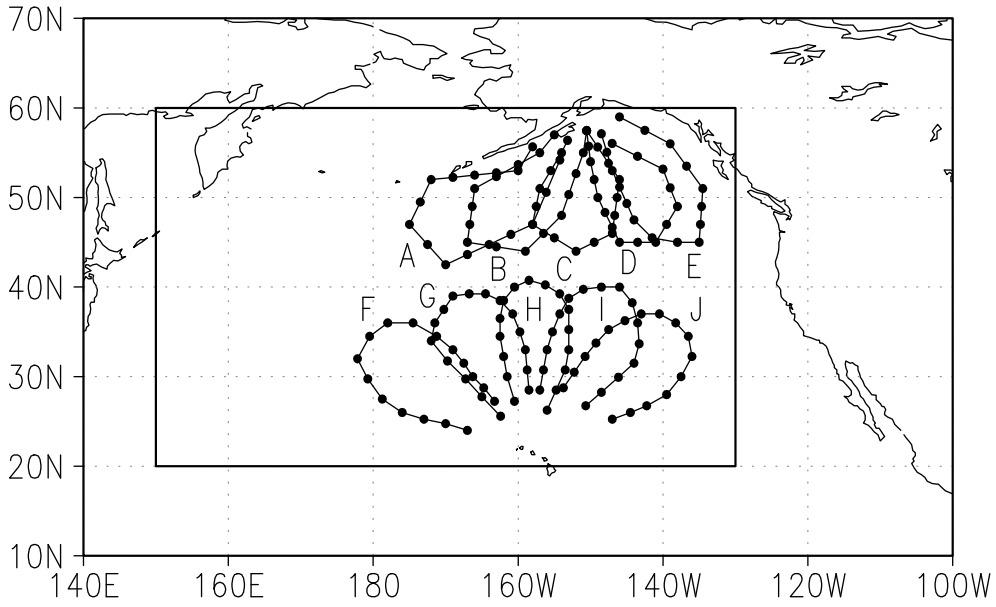

Figure 7: Hypothetical dropwindsonde locations along flight tracks, similar to those used during the 2000 and 2001 Winter Storm Reconnaissance programs. The inner rectangle represents the domain within which the calculations of common locations of ET KF and ECMWF TESV targets were performed. Tracks A, B, C, D, E are deployed from Anchorage, and tracks F, G, H, I, J are deployed from Honolulu.

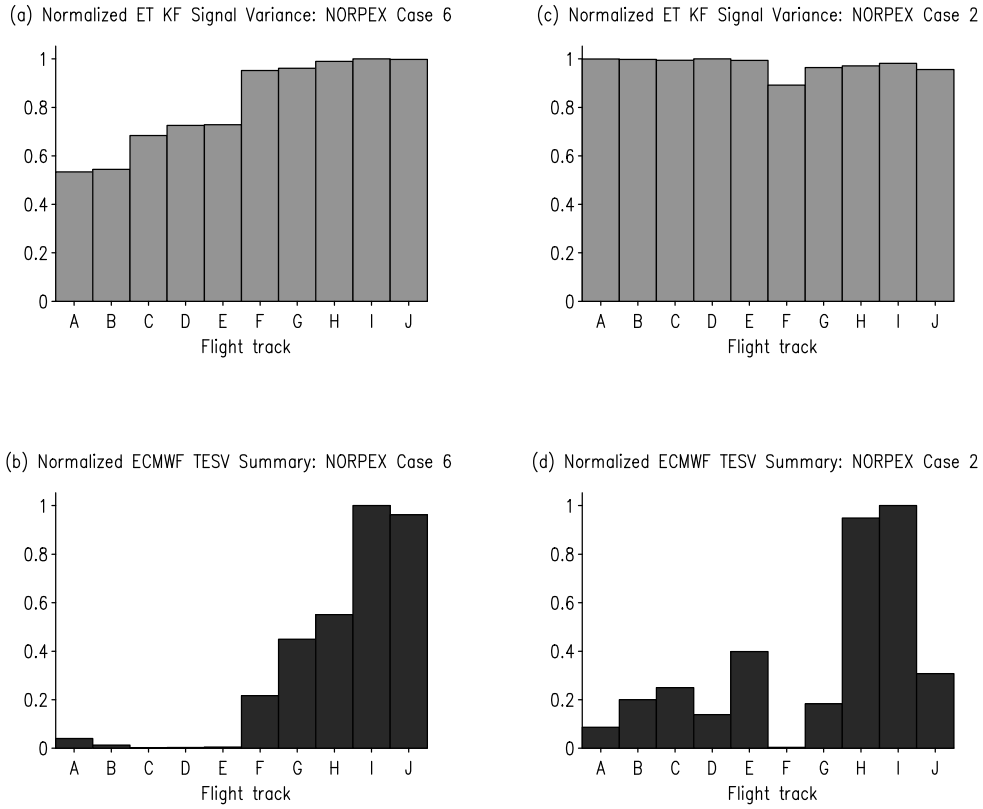

Figure 8: Bar charts showing normalized ET KF and ECMWF TESV summary values for flight tracks A through J, for NORPEX cases 6 and 2. Values are normalized with respect to the maximum value.